DroneVLC

Exploiting Drones and VLC to Gather Data from Batteryless Sensors

de Groot, Lucan; Xu, Talia; Zuniga Zamalloa , Marco

DOI
10.1109/PERCOM56429.2023.10099247

Publication date
2023

Document Version
Final published version

Published in
Proceedings of the 2023 IEEE International Conference on Pervasive Computing and Communications (PerCom)

DroneVLC: Exploiting Drones and VLC to Gather Data from Batteryless Sensors

Lucan de Groot
Delft University of Technology
Lucan.deGroot@gmail.com

Talia Xu
Delft University of Technology
M.Xu-2@tudelft.nl

Marco Zúñiga Zamalloa
Delft University of Technology
M.A.Zunigazamalloa@tudelft.nl

2023 IEEE International Conference on Pervasive Computing and Communications (PerCom) | 978-1-6654-5378-3/23/$31.00 ©2023 IEEE | DOI: 10.1109/PERCOM56429.2023.10099247

***Abstract*—We explore a new alternative for drones to gather information from sensors. Instead of using the traditional radio-frequency spectrum, whose broadcast nature makes it more difficult to poll *specific* objects, we utilize the light spectrum. In our system, the drone carries a light, and flies to an area that it is interested in polling. Only the sensor (tag) under the coverage of the light sends data back by backscattering the impinging light waves. Enabling this system poses two challenges. First, a reliable modulation method with light is required. The method must overcome noise dynamics introduced by the drone (mechanical oscillations), the object (backscattering effects) and the environment (interference from ambient light). Second, to facilitate the deployment of tags in pervasive applications, the design of the tag should be battery-less and have a small surface area. These requirements limit the amount of power available for reception, transmission and sensing, since the energy harvested by solar cells is proportional to their surface area. Regarding the first challenge, we show that the amplitude-based modulation methods used in state-of-the-art studies do not work in our scenario, and investigate instead a frequency-based approach. For the second challenge, we optimize the computation, reception and transmission of the tag to create a battery-less design that operates with frequency-modulated signals generated from light. We build a prototype for the drone and the tag, and test them under different lighting scenarios: dark, indoors, and outdoors with sunlight. The results show that, under standard indoor lighting, our system can attain a polling range of 1.1 m with a data rate of 120 bps, while the tag operates with small solar cells and consumes less than 1 mW.**

***Index Terms*—Visible Light Communication, Backscatter, Batteryless, Drones, UAV, Dynamic Channel**

I. Introduction

Drones are becoming increasingly pervasive in our environments, with many industrial applications exploiting them for precision agriculture, package delivery, and warehouse management, to name a few [1], [2]. An application that is particularly on the rise is monitoring and sensing. For example, barcodes placed on objects are read by the drones' camera [1], or wireless tags embedded on the objects are polled by the drones via RFID [3], [4]. Cameras and radio-frequency (RF) transceivers are reliable technologies to use with drones, but they have a few shortcomings. Cameras raise various concerns about privacy, and their use is one of the main factors limiting a wider acceptance of drones among the general public [5]. On the other hand, RF transceivers are operating on an increasingly congested spectrum [6], and unless a complex antenna design is used, the inherent broadcast nature of RF transmissions makes it harder to poll specific objects.

Vision. We propose an alternative approach to poll objects using light. The basic idea is depicted in Figure 1. A drone carries an LED for transmission, and a photosensor (PD) for receiving signals. To start, the drone points its light towards an area it is interested in polling, and sends a request by modulating the intensity of the light[1]. A tag, which is in an area covered by the light beam, decodes the request, and reuses the light beam to transmit its sensor data to the drone by backscattering (reflecting) the impinging light back to the drone. To allow a pervasive deployment of the tags, their design has to be (i) small, to allow an easy integration to the environment; and (ii) batteryless, to reduce maintenance requirements and the pernicious effects that batteries have on the environment. The above approach does not require cameras and has the advantage of exploiting the visible light spectrum, which is free to use and empty. Furthermore, since drones have inertial sensing units to know their own orientations, and LEDs have a constant field-of-view, a drone will be able to select the area to be polled. Only the tags present under the coverage of the light will respond to the drone.

Challenges. Establishing a bi-directional link between a drone's light and batteryless tags faces unique challenges.

First, attaining a stable communication link. Our work is inspired by pioneering contributions in the area of backscattering communication with light (BCL), where bi-directional links are established between LEDs and tags. Those studies, however, establish links between static points [7], [8], or between a mobile point (person or car) and reflective tags [9], [10]. These scenarios have either zero- or one-degree of freedom, which allows maintaining a more stable link. In our case, the movements of a flying drone create greater link oscillations (distortions) due to the 6-degrees of freedom it has.

Second, designing a batteryless tag. The batteryless tag has to rely only on the power harvested by small solar cells to perform reception, transmission and sensing. This requires a careful design of the tag, as only a limited amount of energy, which varies depending on the ambient light conditions, is available for the tag to perform its operation. The limited energy *harvesting* capabilities (i.e. the small area of the solar

[1]We exploit the principle of visible light communication (VLC) [6], which requires a modulation speed that is high enough to prevent flickering effects. VLC is invisible to the human eye. Even though the LED is modulated, people only see a normal light beam.

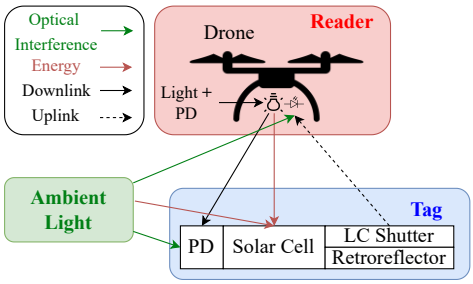

Fig. 1: The system components of DroneVLC.

cells) and the limited energy *storage* capacity (i.e., the use of a supercap instead of a battery), pose a major challenge to perform the required operations for a tag to communicate via light reflections with the drone.

Contributions. This work investigates a challenge at the intersection of three research areas: drone monitoring, visible light communication (VLC), and batteryless design. Overall, we provide the following three contributions.

Contribution 1: A stable communication link for a bi-directional drone-tag communication [Section III]. We show that the *amplitude* modulation scheme used in the state-of-the-art studies (SoA) for backscattering links does not perform well in our setup. This scheme is prone to errors due to the interference caused by the drone's movement. Our design shows that despite its higher complexity, *frequency* modulation provides a reliable link.

Contribution 2: A batteryless tag that performs reception and transmission with less than 1 mW. [Section IV]. We present a detailed framework to reduce the power consumption of the tag by an order of magnitude. The design optimizes the tasks related to processing, transmission and energy harvesting. To the best of our knowledge, this is the first batteryless tag that operates with frequency-modulated signals based on light.

Contribution 3: An evaluation of the system under different lighting conditions [Section V]. We build a prototype for the drone and tag, and evaluate them in both indoor and outdoor conditions under different ambient light intensities. Utilizing a low-power LED (0.5 W), our results show that the system achieves an effective polling range of 1.1 m in standard indoor illumination scenarios.

II. Background and System Overview

In this section, we describe the components of our system and explain how they work together to establish a link between drones and batteryless tags. In addition, we provide an overview of the most relevant research areas and highlight the differences between DroneVLC and those studies.

A. System Overview

The key idea in our system is to use a single LED light, carried by the drone, for both downlink (drone-to-tag) and uplink (tag-to-drone) communication. An overview of our system, DroneVLC, is shown in Figure 1. It has two main devices: a *reader* and a *tag*. The reader is a custom light fixture, which is mounted on the drone. The reader sends commands to the tags to collect data. The downlink communication is achieved by turning an LED on and off rapidly. The modulated light emitted by the LED is decoded using a photodiode (PD) on the tag. Once the commands are received and processed by the tag, the data collected by the sensors on the tag is sent back to the drone through the uplink. Producing the uplink is more involved. Since the tag is batteryless, it cannot generate its own light or radio signals. Instead, the tag uses the light emitted by the drone to backscatter its data. This backscattering process requires two components: A *retroreflector* and a *liquid crystal (LC) shutter*. A *retroreflecter* reflects the received light towards the direction of the light source [7]–[11], while an *LC shutter* modulates the light incident on its surface by becoming transparent or opaque when a voltage is applied to it, blocking or letting light thought its surface. The tag is then able to modulate information by changing the intensity of the light reflected toward the transmitter. In section III-A, we evaluate different retroreflectors and LC shutters to select the ones that are best suited for our system.

In addition to the components for communication, the tags are equipped with a small solar cell to harvest energy from the environment. In DroneVLC, the tags are powered by ambient light only. During the day, the tag is able to harvest energy from the sun. However, at night, since the ambient light might be insufficient to power the tag, the light carried by the drone can also be used to power it.

B. State-of-the-art Studies

1) Gathering data with drones: Drones are used to gather data from the environment due to their ability to move in areas not easily accessible or covered by humans. A widely adopted method to scan the environment is to use cameras. For example, in agricultural and warehouse management, cameras are used to gather various metrics to estimate soil quality and vegetation health or to keep track of inventory and their locations [15]–[18]. However, cameras can cause privacy concerns, which have become an obstacle in allowing camera-equipped drones to gain a wide acceptance in the general public [5]. Other studies use RF signals to gather data from the environment. For example, RFID tags can be used to determine the remaining shelf-life of perishable goods or inventory information [3], [4]. The main disadvantage of RF-based communication is the inherent broadcast and anisotropic nature of RF antennas, making them communicate in all directions at once.

2) Communication with light: The disadvantages of camera and RF-based communication can potentially be overcome by the adoption of VLC. Unlike cameras, visible light communication does not reconstruct images or videos of the environment. Compared to RF signals, light is highly directive, allowing drones to communicate with only the devices of interest, instead of broadcasting their requests. A summary of the most relevant studies in VLC is shown in Table I. Most studies in VLC, however, consist of a static transmitter and receiver, and require a precise alignment between them [19]. For systems with mobile transmitters or receivers, a number of studies have explored vehicle-to-vehicle and vehicle-to-

TABLE I: Comparison of DroneVLC with related works.

Name	Power source	Modulation	Ambient light	FoV	Data rate		Range	Movement	Tag power
					Downlink	Uplink			
Luxlink[12]	Ambient light	Frequency	150 - >70 klx	1°	1 kbps	No Uplink	2.5 m	Static	42 mW[1]
RetroTurbo[8]	4W Flashlight	Amplitude	20 - 1klx	20°	N/S[3]	8 kbps	7.5 m	Static	800 µW[1]
RetroVLC[7]	12W LED	Amplitude	10[2]- 300lx	50°	10 kbps	500 bps	2.4 m	Static	184 µW
PassiveVLC[9]	3W Flashlight	Amplitude	10 - 2klx	4°	2.5 kbps	1 kbps	1 m	Walking (1m/s)	152 µW
RetroI2V[10]	30W Headlight	Amplitude	10[2]- >10klx[2]	30°	5 kbps	1 kbps	80 m	Driving (19m/s)	N/S[13]
AmphiLight[13]	103mW laser	Amplitude	3lx - 73.9klx	Variable	5 Mbps	No Uplink	6.1 m	Drone (Hovering)	623 mW[1]
Sunflower[14]	133mW laser	Frequency	500lx - 10klx	40°	N/S[3]	N/S[3]	3.3 m	Drone (Hovering)	2 W[1]
DroneVLC	0.5W LED	Frequency	10 - 2klx	35.5°	2.5 kbps	120 bps	1.1 m	Drone (Hovering)	881 µW

[1] These works are not operating batteryless.
[2] Estimated from description.
[3] Not specified.

infrastructure communication. For example, RetroI2V [10] enables infrastructure-to-vehicle communication between road signs and cars. However, compared to drones, cars have a much larger body and smooth motions. They do not suffer from the oscillations a small drone would in flight. Lastly, a few studies have looked at the intersections of VLC and drones in underwater communication [13], [14]. Sunflower, in particular, is relevant to our work because they use drones to localize underwater robots using backscattering links. Sunflower, however, uses lasers and a complex set of optical front ends at the drone and under-water robots to maintain the bi-directional link.

3) Backscattering RF Signals: A similar concept to backscattering with visible light is used with ambient RF signals for communication. Previous studies have explored the use of various RF signals, such as TV tower, WiFi, BLE, and LoRa, to establish data links over various data rates and ranges [20]–[22]. RF backscattering is a promising area, but it suffers from the broadcasting nature of RF signals, making it difficult to communicate with *specific* devices. In addition, simple antenna designs typically have a limited bandwidth, meaning that only a narrow RF spectrum can be used for each system.

III. Communication

The link design has two components: downlink and uplink. The downlink, from the drone to the tag, is simpler to implement because it uses an LED and photodiode. The uplink operation, from the tag to the drone, is more challenging due to two reasons. First, the liquid crystal shutter is more complex to control than an LED, and second, the light beam has to travel twice the distance since it is backscattered, and this longer distance creates a stronger attenuation.

Since there is a myriad of studies achieving LED-to-PD communication (downlink in our system) [23], [24], the focus of this section is on the uplink design. First, we analyze and select the most suitable LC cells and retroreflector. Then, we showcase the limitation of the de-facto SoA modulation method and propose a more reliable approach. After that, we provide the details for the message encoding and decoding.

A. Hardware Analysis

As stated before, the uplink requires a retroreflector and LC shutter. A wide assortment of these components is available, and not all products perform the same. Next, we evaluate what retroreflector and LC shutter are best suited for our system.

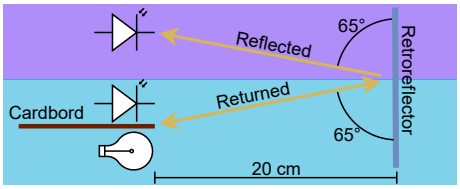

Fig. 2: The evaluation setup used to test (retro)reflectors.

1) Retroreflector: There is no standard for reflective surfaces in the literature. Some studies use retro-reflective fabrics [7]–[10], other works use corner cubes [25], [26], or mirrors to establish directional communication [11], [27].

To determine what reflective surface is best for our system, we execute a small experiment. Two photodiodes are placed facing the reflective surface with an incident angle of 65°, as shown in Figure 2. One photodiode is collocated with an LED, and the received (backscattered) light is labeled 'returned'. This setup captures the scenario faced by the drone. The light received by the other photodiode is labeled 'reflected'. This reflected light cannot be captured in our scenario. The LED modulates its intensity at 150 Hz and the received signals at each photodiode are measured using the Fourier transform. The received signal strength is divided by the total area of the reflector to normalize the results.

Table II shows the materials used and their respective surface area, and Figure 3 presents the results. The corner cube is the best retroreflector with a magnitude above 50, followed by the bike's reflector and the 3M fabric, with magnitudes around 8 and 5, respectively. The corner cube and bike reflectors, however, are not well-suited for our scenario because they are big 3D devices that are hard to reshape to fit the LC's size. Moreover, the corner cube has a narrow FoV, which would require a precise alignment between the drone and the tag. Thus, in our prototype, we use the 3M fabric because it is simple to manipulate and has a wider FoV. This material is similar to the one used in the SoA studies that we consider as baselines [7]–[10], which will allow a fair comparison of the modulation methods. We also test an LC in this setup, which shows some reflective properties, c.f. last column of Figure 3. The LC's reflection will reduce the uplink SNR slightly when the angle is not perpendicular.

2) LC shutter: There is a wide selection of LCs with very different properties. As pointed out in LuxLink [12], the modulation frequency can vary between 20 Hz and 147 Hz,

TABLE II: Evaluated Reflectors.

Reflector	3M Tape 983-10	3M Fabric 8906	Brand A Tape	Brand B Tape	Bike Reflector	Brand C Corner cube	Mirror	LC
Area [cm^2]	56.1	53.56	45.6	41.86	20.16	7.98	61.75	137.75

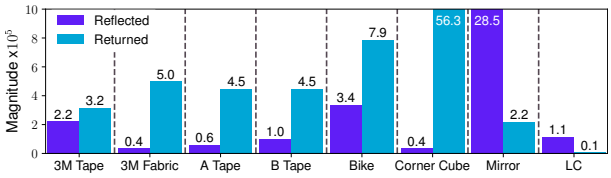

Fig. 3: Results of the reflectivity test.

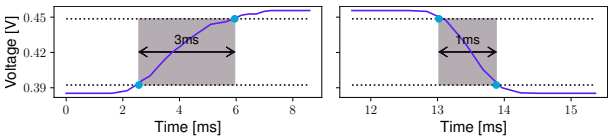

Fig. 4: The rise and fall times of an LC shutter.

depending on the model and driving voltage. The same study shows that the rise (t_{rise}) and fall (t_{fall}) times have different duration, leading to asymmetric pulses that can be hard to modulate. An example of the rise and fall times of an LC driven at 5 V and 60 Hz is given in Figure 4. Note that the response time is ∼4 ms, making the uplink severely bandwidth limited (250 Hz). Moreover, the rise time is three times longer than the fall time, making the pulses highly asymmetrical.

To select the best shutter, we analyze four LCs considering their response time ($t_{rise} + t_{fall}$) and symmetry ($\frac{\max(t_{rise},t_{fall})}{\min(t_{rise},t_{fall})} - 1$). The driving voltages are 3.3 V and 5 V. Table III shows the tested shutters, and Figure 5 provides their performance. The 3D and square shutters perform best in both response time and symmetry. And, at both voltages, the square shutter is faster than the 3D shutter, and thus, we use them in our work. The higher asymmetry of the square shutter at 5 V will be solved next with duty-cycling techniques.

B. Selecting a suitable modulation technique

As mentioned before, our application is motivated by RetroI2V, a pioneering work that proposes a backscattering link between a 30W LED placed on a car and retro-reflecting signs on the road [10]. Since our study also tackles a link between a mobile element (a drone carrying an LED) and tags, one may think that we could use the same modulation technique as RetroI2V. We will show that that is not the case due to the noise introduced by the drone's oscillations.

1) Baselines from the state-of-the-art: To position our work, it is important to discuss in detail two SoA studies. One is based on amplitude modulation (PassiveVLC, [9]), and the other on frequency (LuxLink, [12]).

Amplitude-based modulation: RetroI2V uses the modulation method proposed in PassiveVLC [9]. PassiveVLC has two main components: *(i) Miller coding*, which is a well-known and efficient method to break long sequences of 0's and 1's; and *(ii) Trend-based modulation*, which instead of checking if the received signal is above a threshold to classify the symbol

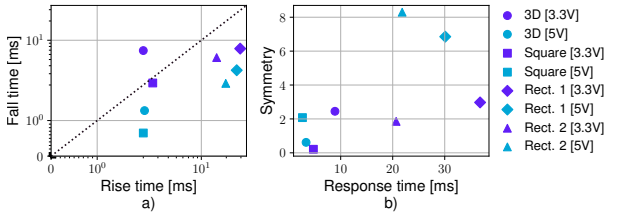

Fig. 5: Analysis of four different LC shutters at 3.3V and 5V. a) The rise and fall times. b) The response time compared to the symmetry of the edges.

TABLE III: Overview of the selected shutters. ‡At 200Hz and 5V † Due to the small size, two shutters are used.

LC	Driving current‡ [µA]	Area [cm^2]
Rect. 1 [28]	54	35.2
Rect. 2 [29]	85	42.8
3D [30]	43	27.2†
Square [31]	45	24.6†

as a one, it checks the signal's trend: if the slope is positive for a period τ, the symbol is deemed to be a one.

Trend-based modulation is designed to overcome the slow rise time of LC cells. Instead of waiting until a plateau is reached, earlier symbol decisions are made based on the slope. The drawback is that since the decisions depend on smaller changes in amplitude, the approach is more sensitive to noise.

Frequency-based modulation: Luxlink designs a passive link that works outdoors with sunlight [12]. The transmitter and receiver are static, but the method considers the changes in sunlight intensity during the day. Their design uses frequency-shift keying (FSK) and relies on LCs with similar rise and fall times to generate stable signals with different frequencies.

Frequency modulation is, by design, resistant to changes in the signal's amplitude, but (i) has higher bandwidth requirements, (ii) requires a more complex transmitter and receiver, and (iii) considering our LCs, it would need to overcome the asymmetry of the rise and fall times to generate stable frequencies.

What modulation method is better? Overall, the SoA presents two options that tackle different types of dynamics. An amplitude-based method that considers a *mobile object*; and a frequency-based method that copes with *temporal changes in sunlight*. Next, we evaluate these two methods and show that the frequency-based approach is more reliable.

2) Tackling link asymmetry: The asymmetry of LC signals affects amplitude- and frequency-based approaches. Figure 6 shows Miller and 4-FSK modulated signals by an LC. The slow rise time leads to distorted signals with both approaches, but the effect is more dramatic on FSK because, as the frequency increases, the signal stops being modulated (becoming a flat line).

To ameliorate this issue, we propose using a duty-cycled

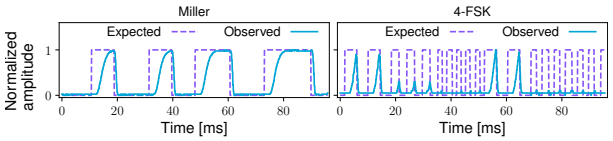

Fig. 6: Default Miller and 4-FSK encoded messages.

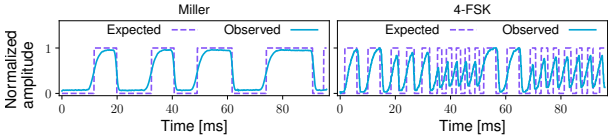

Fig. 7: Enhanced Miller and 4-FSK encoded messages.

signal. Instead of giving the same amount of time to both edges, we give *less time* to the *fast* falling edge and *more time* to the *slow* rising edge. Figure 7 shows the same Miller and 4-FSK encoded messages, but with a $16.67\,\%$ duty cycle, instead of the $50\,\%$ one[2]. Note that even after reducing the asymmetric issue, the amplitude of the 4-FSK symbols decreases as the frequency increases. This occurs due to the low bandwidth of LCs. As the frequency increase, the amplitude reduces, until reaching eventually a flat line (approximately at $1000\,\mathrm{Hz}$). However, while this reduces the SNR of high-frequency symbols, it does not affect the performance dramatically, since the signal is decoded based on the frequencies, not the amplitude.

3) Flight dynamics and ambient interference: The photodiode in the drone will be exposed to two dynamics: changes in ambient light and the mechanical movement of the drone. The interference created by ambient light is either constant (indoors) or may have only slow changes (outdoors). In these cases, the interference may be easy to filter because it appears as a DC-offset. But if the frequency spectrum of the interference overlaps the signal's spectrum, the decoding may not be possible. This latter case is what happens due to the drone's dynamics, as we will see next.

Effect of drone's dynamics: Figure 8 shows the measurements of the drone's photodiode while hovering *in-place* in an indoor scenario with a *constant* ambient light of $300\,\mathrm{lx}$. Even in this benign scenario, hovering under constant light, the interference shows mostly low-frequency noise ($<20\,\mathrm{Hz}$), which will overlap with the spectrum of the signal modulated by the tag (LC). The peak-to-peak change in this signal is $275\,\mathrm{mV}$, which is $12\,\%$ of the photodiode's dynamic range.

Effect on amplitude modulation: Figure 9 shows a Miller encoded message imposed on a randomly selected sample of ambient noise from Figure 8. To remove the ambient noise, the message can be filtered. While a second-order Butterworth filter with a cutoff frequency at $1\,\mathrm{Hz}$ can remove the DC offset, there is still low-frequency noise present. If the cutoff frequency is increased to $20\,\mathrm{Hz}$, the low-frequency noise is removed, but the signal gets severely distorted in the process. This occurs because the spectrum of amplitude modulated

[2]Implementing the duty-cycle technique in FSK is relatively simple, but it is more complex for Miller because of the pre-defined symbol periods (1x, 1.5x, 2x). Due to space constraints, we do not provide all the required details.

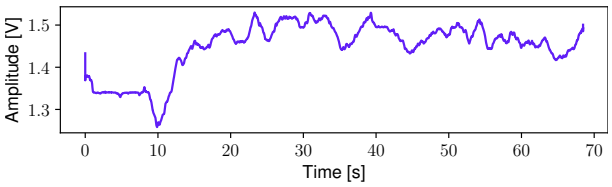

Fig. 8: Recording of the channel at a reader mounted on a drone that is hovering under constant ambient light.

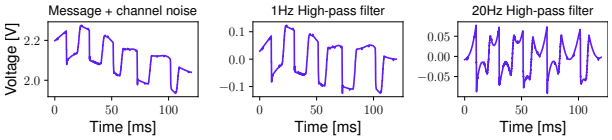

Fig. 9: The effect of high pass filters on a Miller encoded message with ambient channel noise.

signals is inherently wide, as shown in the Power Density Spectrum (PSD) of Figure 10. Thus, filtering out the noise also distorts the sharp edges.

Effect on frequency modulation: The low-frequency noise has little effect on M-FSK signals because the PSD focuses on the modulation frequencies ($f_i ... f_{M-1}$), as shown in Figure 10. In fact, for the 4-FSK signal, $34.6\,\%$ of all power is concentrated within the four modulation frequencies ($\pm 5Hz$), leading to peaks that have SNRs of 21 dB. Therefore, the frequency spectrum of the drone's dynamics will not degrade significantly the link's quality. On the other hand, $80.8\,\%$ of the Miller signal power is concentrated before $60\,\mathrm{Hz}$ — even though the critical frequencies are 120, 90 and $60\,\mathrm{Hz}$.

4) Summary: The modulation proposed in PassiveVLC, and used in RetroI2V, is valuable but considers relatively stable interference (ambient light level). Under those conditions, amplitude-based signals perform well because DC-offsets are simple to filter. Drones, on the other hand, introduce higher frequency noise with a spectrum that overlaps the bandwidth of LC shutters. To overcome this situation, we build a frequency-modulation method inspired by LuxLink. Contrary to that work, however, which uses slower but symmetric LCs in scenarios with slow-changing sunlight, we propose a method that works with the higher frequency noise generated by drones using faster but more asymmetric LCs, and overcome the asymmetric limitation with a duty-cycling scheme.

C. Implementation

1) Modulation: We use coherent M-FSK for the down- and up-link with the parameters presented in Table IV.

2) Demodulation: The receiver knows the preamble used by the transmitter and demodulates the message as follows.

Message detection: Since the reader (drone) has more resources, it uses a matched-filter to detect the frequencies in the preamble. The tag, which is resource-constrained, uses a simple Fourier Transform (FFT).

Message decoding: On the reader, a message is buffered on the microcontroller before being decoded by four matched-filters and envelope detectors tuned to the symbol rate. For

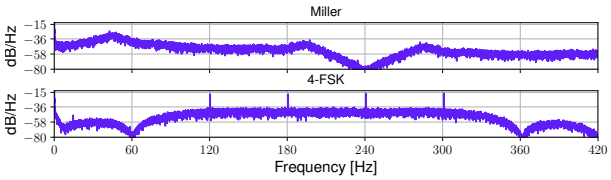

Fig. 10: The PSD of randomly generated Miller and 4-FSK signals at 120bps superimposed on the noise from Figure 8.

TABLE IV: Overview of the communication parameters between the reader and tag.

Parameter	Tag	Reader
M	4	2
Frequencies [Hz]	120, 180, 240, 300	5000, 7500
Data rate [bps]	120	2500
Decode method	Fourier transform	Matched filter

the tag, a message is decoded in real-time by continuously applying FFTs until the entire preamble and data are decoded.

IV. Moving Towards a Batteryless Design

In the previous section, we show that the use of frequency-based modulation is necessary to establish a stable link with a flying drone. However, compared to amplitude-based modulation schemes, frequency-based modulation consumes more power and is more complex to decode [7], [9]. Previous *batteryless* VLC backscattering systems employ the use of amplitude-based modulation schemes [7], [9], while systems employing frequency-based modulation schemes still require batteries to operate [12], [14]. DroneVLC is the first work that combines a frequency-based modulation scheme with a batteryless tag. In this section, we describe how we design our system to operate in a batteryless manner.

A. Low-Power Hardware Design

The hardware implementation of our prototype is shown in Figure 12. Since the tag is powered by only ambient light, low-power components are chosen for the prototype. We use an array of six AnySolar SM101K07L solar cells with a total area of $46.2\,\mathrm{cm}^2$. A small solar cell area is chosen to keep the tag compact. The harvested energy is managed by the Lightricity 4EverLast3.0 harvester IC, which allows us to start harvesting energy at a light intensity lower than 200 lux [32]. Using the same power estimation as [11], these solar cells can provide $0.4\,\mathrm{mW}$ at $300\,\mathrm{lx}$ and $2.7\,\mathrm{mW}$ at $2000\,\mathrm{lx}$. The harvested energy is stored in three $220\,\mu\mathrm{F}$ electrolytic capacitors connected in parallel. The harvester IC provides two power rails, $1.8\,\mathrm{V}$ and $3.3\,\mathrm{V}$. The $1.8\,\mathrm{V}$ power rail is used to power the Silicon Labs BGM220P microcontroller. The $3.3\,\mathrm{V}$ is used to provide power to the PD for receiving signals, and also to generate a 5V signal by connecting to a TI TPS61099 DC-DC converter, which modulates the LC shutter for backscattering. With our baseline implementation, we measure the power consumed by the tag over a two-second time period, during which the reader and the tag communicate once. To measure a detailed power profile, we use the Advanced Energy Monitor incorporated with the development kit from Silicon Labs. The baseline

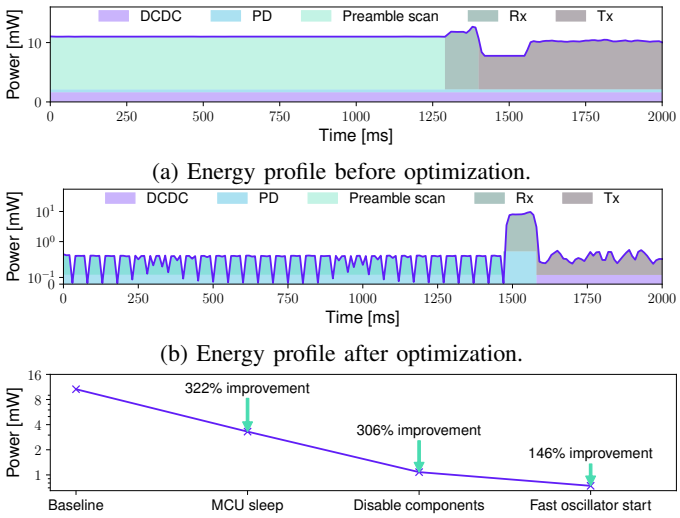

(a) Energy profile before optimization.

(b) Energy profile after optimization.

(c) Energy improvement.

Fig. 11: Energy profile and improvement of the tag.

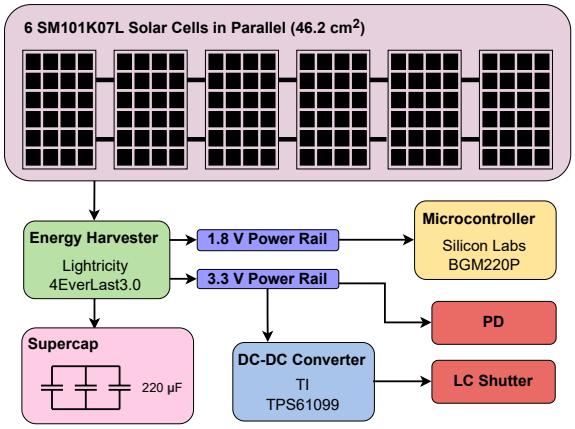

Fig. 12: Hardware implementation of the tag.

implementation consumes 10 mW on average, and the detailed power profile is shown in Figure 11a. This is much higher than the energy that we are able to harvest from the solar cells, therefore, in the next section, we look at methods to reduce power consumption.

B. Achieving batteryless performance

The key to reducing the power consumption further is to enable components only when they are in use. There are two main aspects: putting the MCU to deep sleep mode whenever possible, and disabling any peripheral hardware when they are not in use.

1) Putting the MCU to sleep: Our tag design puts the MCU to sleep during part of the preamble scan (reception) and the backscattering process (transmission).

Preamble scan: In this state, the tag tries to detect the presence of drone signals. Once it is detected, the tag will start receiving and decoding the command, and backscattering a response. It is shown in Figure 11a that the preamble scan lasts the longest and consumes the highest amount of energy.

This is because the tag needs to be active in this state to read and decode the preamble, which arrives at unpredictable times. However, since only a small portion of the preamble needs to be captured, we can modify our tag to only wake up periodically to check for the presence of a preamble[3]. If the preamble length is t_{pream}, then we only need to scan every $\frac{t_{pream}}{2}$ to still capture the preamble. The preamble transmitted by the reader is 50 ms long, by scanning for just 2 ms at 23 ms intervals (where we enter deep sleep for the rest of the time), we can save considerable power, while still consistently detecting the preamble.

Backscattering (TX): For each symbol the tag sends to the drone, the modulation frequency stays the same for the duration of the symbol. To save power in the TX state, we set the MCU to sleep once the modulation frequency for a symbol is written to the PWM. This allows the MCU to stay idle and only become active at the beginning of a symbol change.

The use of periodic wake-ups for reception (preamble) and transmission (backscatter) reduces the average power to 3.3 mW (322% improvement).

2) Disabling components not in use: There are circuits on the tag that are dedicated to certain operations. For example, the DC-DC booster is only used in the transmitting (TX) state, and the PD is only used in the receiving state (RX) and preamble scan. By disabling the circuit components when they are not in use, we are able to reduce the average power to 1.08 mW (308% improvement).

3) Optimizing register access pattern: In order to overcome the asymmetric rise and fall time of the LCs, we need to change the duty cycle of the driving signal, as discussed in III-B2. This requires us to use the PWM for transmission. To start transmitting with the PWM (after the receiving state), the timer needs to be initialized. However, the timer operates in the low-frequency domain and this process blocks certain registers while they are synchronized between the different frequency domains. By optimizing the write patterns to these registers, such that we do not need to wait for synchronization, we are able to improve the initialization time from 163 ms to 21 µs, and reduce the power consumption to 0.88 mW (123% improvement).

C. Summary

The final energy profile is shown in Figure 11b and Table V. With the proposed hardware and software optimizations, we are able to improve the tag's energy consumption from over 10 mW to 0.88 mW. This makes it possible to operate the tag with only the harvested energy provided by a small solar cell array of 46.2 cm^2. Compared to other low-power VLC backscattering systems that employ frequency-based modulation schemes in the SoA, which consume between 42 mW to 2 W, DroneVLC consumes power that is an order of magnitude lower [12], [14]. RetroVLC and PassiveVLC achieve a lower power consumption on the tag, but these systems use amplitude-based modulation schemes, which inherently can be decoded more efficiently than frequency-based modulation [7], [9]. In addition, RetroVLC and PassiveVLC were evaluated under static or walking scenarios, which do not suffer from the high-frequency noise components introduced by the oscillations of the drone when flying, making filtering and decoding simpler. To cope with the noise in drone-tag communication, DroneVLC adopts a more reliable frequency-based modulation scheme, which consumes more power for communication, then optimizes the system design to achieve batteryless operation. In future work, we plan to further reduce the power consumption by offloading part of the processing from the MCU to dedicated analog modules.

[3]We borrow this periodic wakeup approach from the area of wireless sensor networks, which used it widely to improve the performance of the Medium Access Control Layer for low power operation [33]

TABLE V: An overview of the system power consumption at 3.3 V from Figure 11b.

State	Scan		Rx		Tx		Average		Total
Part	MCU	PD	MCU	PD	MCU	LC	MCU	HW	
Power [uW]	403	184	6880	710	18.9	378	613	268	**881**
Energy [mJ]	528	241	688	71	11	223	1227	535	**1762**

TABLE VI: Parameters of the different evaluation scenarios.

Parameter	All possible values		Baseline values	
	tag	reader	tag	reader
Distance [cm]	25 - 200		100	
Ambient Light	Dark/Ambient/Outside		Ambient	
Scenario	Powered/ Batteryless	Static/ Dynamic	Powered	Static

† For the outside environmental lightning, the gain is reduced to prevent saturation.

V. Evaluation

The prototypes built to evaluate DroneVLC are shown in Figure 13. In our evaluation, we consider two effects, the batteryless operation of the tag and the mobility of the drone. To isolate and quantify the individual effects, we evaluate our system in three steps. First, we evaluate the *baseline* performance, where the reader is static and the tag is externally powered. Next, we evaluate the link reliability when the tag operates *batteryless*. With the batteryless operation, we consider two scenarios, first when the drone is *static*, and second when the drone is *flying* in front of the tag.

To benchmark our system, we evaluate the *communication range* considering the following variations in the setup:

- Ambient light: The intensity of the ambient light as measured on the PD on the tag, we discern three regions : Dark ($<$100 lx), Ambient (100 - 500 lx) and Outside ($>$1000 lx).
- Scenario: For the reader, we consider two scenarios, whether the drone is flying (dynamic) or not (static). For the tag, we utilize two configurations, whether it is operating batteryless or externally powered.

Table VI gives an overview of the parameters considered in our experiments. The *baseline* uses a static drone with a powered tag and a fixed set of parameters, but our overall evaluation considers a broader range of parameters. For the drone, we use the Robomaster TT from DJI. The LED mounted on the drone is 0.5 W.

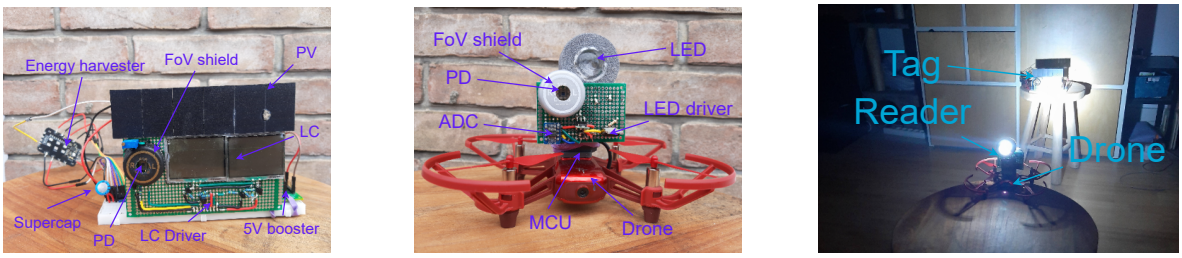

(a) Tag (b) Reader (c) System in the dark

Fig. 13: The DroneVLC prototypes.

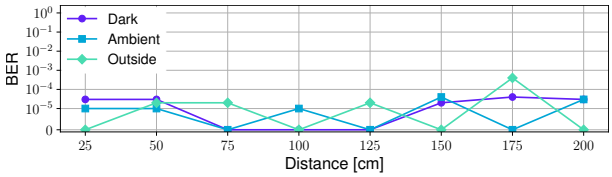

(a) Downlink.

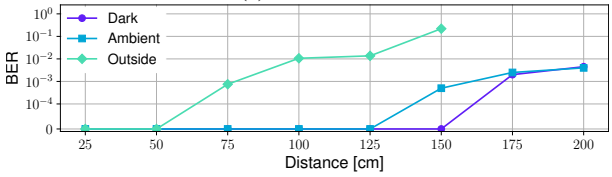

(b) Uplink.

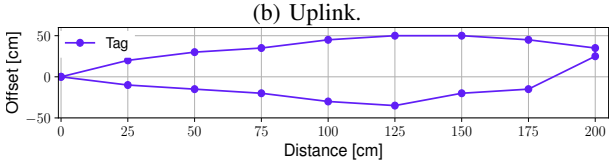

(c) Horizontal offset.

Fig. 14: The bit error rate in baseline scenario.

A. Baseline system performance

We first evaluate the communication distance between the reader and tag in a static and powered scenario. In this experiment, the tag and the reader face directly at each other. The reader has a data rate of 2.5 kbps and sends a query packet of 56 bytes. The tag has a data rate of 120 bps and replies with a packet of 32 bytes. Each transaction is repeated 30 times. Note that backscattering links using LCs are inherently slow, providing rates between 80 bps and 1 Kbps for single-cell transmitters [7], [9]–[12]. Thus, DroneVLC has a competitive backscattering performance. We consider a communication successful when the BER is under 1%, in line with other studies characterizing backscattering links [10].

Figure 14a and Figure 14b show the average BER for *downlink* and *uplink* communication, respectively, for a distance up to 200 cm. The downlink (drone-to-tag) is stable across all ambient light conditions, and the uplink (tag-to-drone) has a BER lower than 1% for up to 200 cm in dark and ambient scenarios. In the experiment conducted outside, the communication range is reduced to 100 cm. This is because the ambient light intensity is stronger, which requires reducing the gain of the PD to avoid saturation. A lower PD gain reduces its sensitivity, resulting in a lower communication range.

It is important to note that the baseline is not a realistic setup, the drone is not flying (static) and the tag is powered, but this controlled setup will allow quantifying the negative effects of mobility and batteryless operation. Furthermore, the baseline scenario allows measuring misalignment effects, as described next.

Misalignment between reader and tag: In addition to the communication range, we need to know how precise the reader and tag need to be aligned. If a precise alignment is required, it will be more difficult for the drone to locate the tag and position itself to establish a link. To analyze *only* the effect of misalignment, we conduct experiments in the dark. The tag is placed in a fixed position and we start by placing the reader right in front of the tag. We then move the reader to the left and right. In Figure 14c, we plot the edge where the BER of the link is less than 1 %. We achieve a working range of 200 cm with a maximum field of view of 35.5°, which indicates that the drone will be able to communicate successfully with the tag even when they are not perfectly aligned.

B. Link reliability in batteryless scenarios

After establishing the baseline performance, we look at the performance when the tag operates batteryless and when the drone is flying. In the following experiments, the transaction success rate (TSR) is used as a metric to determine link quality. A transaction is considered successful if the reader can decode the response from the tag within 10 s of the initial transaction. A successful transaction validated that both the down- and up-link operate correctly. The transaction success rate (TSR) is calculated based on 30 transmissions. We use TSR instead of BER in batteryless scenarios because we cannot log the BER without interacting with the tag, which in turn changes the power consumption. We give the tags a window of 10 s to respond because the capacitors need to store sufficient energy to carry out a complete transaction. A transaction takes 685 ms and the time required to gather the necessary energy can be slow in low illumination conditions. At a light intensity of around 300 lx, which is typical for a dim indoor environment, the tag takes between 5 s and 10 s for the capacitors to accumulate enough energy.

Static batteryless: In the first scenario, the tag operates batteryless, but the reader remains static. Figure 15 presents the TSR. The results show that the system performs best in the ambient scenario, which results in a TSR over 80% for up to 150 cm. In the outside scenario, the communication range

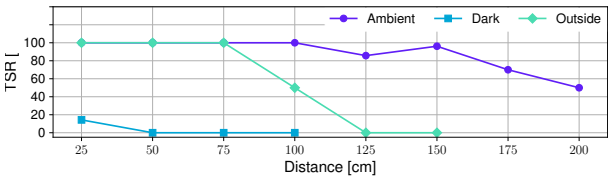

Fig. 15: Transaction Success Rate when the tag is operating batteryless and the reader is static.

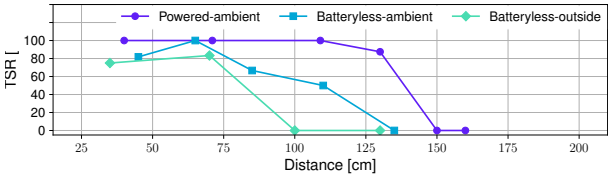

Fig. 16: Transaction Success Rate when the tag is operating batteryless and the reader is dynamic.

drops due to a reduced gain of the PD (similar effect to the baseline result). In the dark scenario, the TSR is low due to the slow charging time of the tag. Since the tag can only rely on the reader's LED power, the drone needs to fly quite close to the tag to provide enough power. Note that we use a low-power LED (0.5 W), a more powerful LED would increase the performance.

Dynamic batteryless: In the second scenario, we operate the tag batteryless and fly the drone in front of the tag using a smartphone as a remote control. Figure 16 shows the results. We carry out one evaluation with the tag externally powered as the baseline for comparison. It can be observed that compared to static scenarios, the communication range of the dynamic scenario degrades further in general. First, we look at the result with the tag externally powered ('Powered-ambient'), which can communicate up to 130 cm. When the system operates batteryless ('Batteryless-ambient'), the TSR drops to around 60% for up to 110 cm. Similar to the previous experiments, the performance when operating outside degrades further, achieving an effective range of around 75 cm.

Noise floor: The previous results show that the communication range degrades when the drone is flying. Since drone mobility is the key and novel dynamic in our work, we investigate this issue further. We evaluate the noise floor of the reader's PD in three different scenarios, as indicated in Table VII: USB-powered and static; battery-powered static; and battery-powered and flying. This analysis shows that the noise floor is higher when the reader is powered by the battery, and especially high when the drone is flying. This occurs because the motors of the drone, the LED light and the PD share the same power source. When the motors and the LED are on, they cause a significant load on the battery, which in turn increases the noise floor of the PD considerably. In future work, we can improve the performance of the system further by adding additional circuit elements to filter out the noise induced by the other components on the drone.

C. Proof-of-concept application

In this section, we consider a proof-of-concept application in indoor monitoring. Specifically, we look at what impact closed and open windows have on the temperature and humidity of a room over time. A batteryless tag is equipped with external temperature and humidity sensors to collect data from the room. A drone periodically flies to the tag and retrieves the data. The drone (reader) initiates the transaction by transmitting a command to the tag. Upon reception of the command, the tag reads the sensor values and transmits a 32-bit frame containing a 16-bit temperature data and a 8-bit humidity data, followed by a checksum (CRC). For this experiment, we first close the windows and doors in a sun-facing room. Then, when the room has warmed up sufficiently, we open the windows and start measuring. We periodically fly the drone in front of the tag to poll it as the room ventilates. After the sensor values have stabilized, we close the windows again. Figure 17 shows the results. We can see that the humidity and temperature drop at the beginning of the tests, when the room is venting. Interestingly, the humidity drops steeply at the beginning, but slowly increases, even when the windows stay open. This could be to the human presence during the test. We close the door and windows at 13:45, and immediately observe that both the humidity and temperature increase afterwards. Over the period of one and half hour, the drone is able to reliably read from the tag.

TABLE VII: Overview of the reader noise floor (standard deviation) in different scenarios when facing a plain white wall.

Scenario	USB-powered	Battery-powered	
	Static	Static	Flying
STD [x1000]	0.23	0.5	1.96

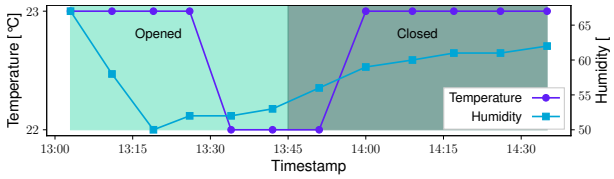

Fig. 17: The temperature and humidity changes in a room as the windows are open and closed.

VI. Conclusion

In this work, we explore the approach of using visible light to communicate between a flying drone and a batteryless tag. First, we design a stable communication link based on frequency-modulation schemes using a single LED light carried by the drone. Second, we optimize the power consumption of the tag to allow it to operate batteryless. Lastly, we build a prototype and carry out a thorough evaluation under different lighting conditions. Our results show that the system can communicate up to 1.1 m with standard indoor lighting conditions.

Acknowledgments

This work has been funded by the European Union's H2020 programme under the Marie Skłodowska Curie grant agreement ENLIGHTEM No. 814215, and by the Dutch Research Council (NWO) with the FIREFLY XS-Grant with project number OCENW.XS21.2.077.

REFERENCES

[1] Y. Almadani, D. Plets, S. Bastiaens, *et al.*, "Visible light communications for industrial applications—challenges and potentials," *Electronics*, vol. 9, no. 12, 2020.

[2] L. Wawrla, O. Maghazei, and T. Netland, "Applications of drones in warehouse operations," *Whitepaper. ETH Zurich, D-MTEC*, 2019.

[3] S. Piramuthu, "Drone-based warehouse inventory management with iot for perishables," in *Smart Services Summit*, 2022.

[4] A. Dimitriou, A. Tzitzis, A. Filotheou, *et al.*, "Autonomous robots, drones and repeaters for fast, reliable, low-cost rfid inventorying & localization," in *SpliTech'21*.

[5] P. Hitlin, "How americans feel about drones and ways to use them," *Pew Research Center*, 2017.

[6] H. Haas, "High-speed wireless networking using visible light," *Spie Newsroom*, vol. 1, no. 1, 2013.

[7] J. Li, A. Liu, G. Shen, L. Li, C. Sun, and F. Zhao, "Retro-vlc: Enabling battery-free duplex visible light communication for mobile and iot applications," in *Proceedings of the 16th Int. Work. on Mob. Comp. Sys. and App.*, 2015.

[8] Y. Wu, P. Wang, K. Xu, L. Feng, and C. Xu, "Turboboosting visible light backscatter communication," in *SIGCOMM'20*.

[9] X. Xu, Y. Shen, J. Yang, *et al.*, "Passivevlc: Enabling practical visible light backscatter communication for battery-free iot applications," in *MobiCom'17*.

[10] P. Wang, L. Feng, G. Chen, *et al.*, "Renovating road signs for infrastructure-to-vehicle networking: A visible light backscatter communication and networking approach," in *MobiCom'20*.

[11] S. Shao, A. Khreishah, and H. Elgala, "Pixelated vlc-backscattering for self-charging indoor iot devices," *IEEE Photon. J.*, vol. 29, no. 2, 2016.

[12] R. Bloom, M. Z. Zamalloa, and C. Pai, "Luxlink: Creating a wireless link from ambient light," in *Proceedings of the 17th Conf on Embedd. Networkd. Sens. Sys.*, 2019.

[13] C. J. Carver, Z. Tian, H. Zhang, K. M. Odame, A. Q. Li, and X. Zhou, "AmphiLight: Direct Air-Water communication with laser light," in *NSDI'20*.

[14] C. J. Carver, Q. Shao, S. Lensgraf, *et al.*, "Sunflower: Locating underwater robots from the air," in *MobiSys'22*, 2022.

[15] A. Eltner, C. Mulsow, and H. Maas, "Quantitative measurement of soil erosion from tls and uav data," *Int. Arch. Photogramm. Remote Sens. Spat. Inf. Sci*, vol. 40, 2013.

[16] M. Ridolfi, N. Macoir, J. Vanhie-Van Gerwen, J. Rossey, J. Hoebeke, and E. De Poorter, "Testbed for warehouse automation experiments using mobile agvs and drones," in *(INFOCOM'19 WKSHPS)*.

[17] *Warehouse drone*, May 2022. [Online]. Available: eyesee-drone.com.

[18] *Infinium scan*, Aug. 2022. [Online]. Available: infiniumrobotics.com/infinium-scan/.

[19] A. H. Azhar, T.-A. Tran, and D. O'Brien, "A gigabit/s indoor wireless transmission using mimo-ofdm visible-light communications," *IEEE Photon. Technol. Lett.*, vol. 25, no. 2, 2012.

[20] V. Liu, A. Parks, V. Talla, S. Gollakota, D. Wetherall, and J. R. Smith, "Ambient backscatter: Wireless communication out of thin air," *SIGCOMM Comput. Commun. Rev.*, vol. 43, no. 4, pp. 39–50, Aug. 2013.

[21] D. Bharadia, K. R. Joshi, M. Kotaru, and S. Katti, "Backfi: High throughput wifi backscatter," Aug. 2015, pp. 283–296.

[22] N. Van Huynh, D. T. Hoang, X. Lu, D. Niyato, P. Wang, and D. I. Kim, "Ambient backscatter communications: A contemporary survey," *IEEE Commun. Surv. Tutor.*, vol. 20, no. 4, 2018.

[23] P. H. Pathak, X. Feng, P. Hu, and P. Mohapatra, "Visible light communication, networking, and sensing: A survey, potential and challenges," *IEEE Commun. Surveys Tuts.*, vol. 17, no. 4, 2015.

[24] L. E. M. Matheus, A. B. Vieira, L. F. Vieira, M. A. Vieira, and O. Gnawali, "Visible light communication: Concepts, applications and challenges," *IEEE Commun. Surveys Tuts.*, vol. 21, no. 4, 2019.

[25] S. Shao, A. Khreishah, and J. Paez, "Passiveretro: Enabling completely passive visible light localization for iot applications," in *INFOCOM'19*, 2019.

[26] S. Shao, A. Khreishah, and I. Khalil, "Retro: Retroreflector based visible light indoor localization for real-time tracking of iot devices," in *IEEE Int. Conf. Intell. Comput.*, 2018.

[27] T. Xu, M. C. Tapia, and M. Zúñiga, "Exploiting digital micro-mirror devices for ambient light communication," in *NSDI'22*.

[28] Pimoroni. "Lcd shutter." (2022), [Online]. Available: shop . pimoroni . com / products / lcd - shutter ? variant = 47109536138.

[29] Adafruit. "Large liquid crystal light valve - controllable shutter glass." (2022), [Online]. Available: adafruit . com/product/3330.

[30] BoutiqueHouse. "2pcs active shutter eyewear." (2022), [Online]. Available: aliexpress . com / item / 1005001469733527.html.

[31] L. C. Technologies. "Lcd shutters." (2022), [Online]. Available: liquidcrystaltechnologies . com / products / lcdshutters.htm.

[32] lightricity. "Power sub-systems." (2022), [Online]. Available: lightricity.co.uk/power-sub-systems.

[33] R. C. Carrano, D. Passos, L. C. Magalhaes, and C. V. Albuquerque, "Survey and taxonomy of duty cycling mechanisms in wireless sensor networks," *IEEE Commun. Surv. Tutor.*, vol. 16, no. 1, 2013.